Journal of Solid State Chemistry 182 (2009) 881–887

Contents lists available at ScienceDirect

Journal of Solid State Chemistry

journal homepage: www.elsevier.com/locate/jssc

Magnetic and charge transport properties of the Na-based Os oxide pyrochlore

Y.G. Shi [a,b,c,*], A.A. Belik [b,c], M. Tachibana [d], M. Tanaka [d], Y. Katsuya [c], K. Kobayashi [d], K. Yamaura [a,c], E. Takayama-Muromachi [a,b,e]

[a] Superconducting Materials Center, National Institute for Materials Science, 1-1 Namiki, Tsukuba, Ibaraki 305-0044, Japan
[b] International Center for Materials Nanoarchitectonics (MANA), National Institute for Materials Science, Tsukuba, Ibaraki 305-0044, Japan
[c] JST, Transformative Research-Project on Iron Pnictides (TRIP), Tsukuba, Ibaraki 305-0044, Japan
[d] NIMS Beamline Station at SPring-8, National Institute for Materials Science, 1-1-1 Kouto, Sayo-cho, Sayo-gun, Hyogo 679-5148, Japan
[e] SPring-8 Service Co. Ltd., 1-1-1 Kouto, Sayo-cho, Sayo-gun, Hyogo 679-5148, Japan

ARTICLE INFO

Article history:
Received 19 November 2008
Received in revised form
6 January 2009
Accepted 8 January 2009
Available online 21 January 2009

Keywords:
$Na_{1.4}Os_2O_6 \cdot H_2O$
Crystal structure
Physical property

ABSTRACT

The Na-based osmium oxide pyrochlore was synthesized for the first time by an ion-exchange method using KOs_2O_6 as a host. The composition was identified as $Na_{1.4}Os_2O_6 \cdot H_2O$ by electron probe micro-analysis, thermogravimetric analysis, and structural analysis using synchrotron X-ray diffraction. $Na_{1.4}Os_2O_6 \cdot H_2O$ crystallizes in a regular pyrochlore structure with some defects (space group: Fd-3m, $a = 10.16851(1)$ Å). Electrical resistivity, heat capacity, and magnetization measurements clearly showed absence of superconductivity down to 2 K, being in large contrast to what was found for the β-type pyrochlore superconductor AOs_2O_6 (A = Cs, Rb, and K). The Sommerfeld coefficient is 22 mJ K^{-2} mol^{-1}, being the smallest among AOs_2O_6. A magnetic anomaly at ~57 K and associated magneto-resistance (+3.7% at 2 K in 70 kOe) were found.

1. Introduction

The pyrochlore superconductor AOs_2O_6 (A = Cs, Rb, and K) attracts many attentions probably because an unusual mechanism coupled with A atom rattling may play a significant role in establishing the superconductivity [1–3]. To date, many studies have focused on the possibility; however, role of the rattling in the superconductivity still remains ambiguous [4–13]. Additional studies are needed to put forward further progress on the issue. Besides, it is suggested that T_c goes up efficiently by replacing the A atom by a lighter element. In fact, superconducting critical temperature (T_c) goes up step by step depending on the A atom mass from 3.3 K (A = Cs) to 6.4 K (Rb), and to 9.6 K (K) [3]. The unsophisticated anticipation may come from a simple picture based on the possible unusual mechanism. In order to deepen understanding of the role of the rattling, we tried to synthesize the pyrochlore AOs_2O_6 with A = Na instated of Cs, Rb, or K. Within our best knowledge, the Na-based pyrochlore was hitherto unattained.

Regarding strongly correlated electrons properties, Os oxides are rich: for example, a ferromagnetic Mott transition was observed in Ba_2NaOsO_6 [14], a metal–insulator transition associated with antiferromagnetic order was found in $Cd_2Os_2O_7$ [15], antiferromagnetic correlations in $Hg_2Os_2O_7$, Na_3OsO_5, and La_2NaOsO_6 [16–19], and spin–flop transitions in Pr_2NaOsO_6 and Nd_2NaOsO_6 are notable [19]. Further development of Os oxides could shed more light on nature of the correlated 5d electrons properties, and would be helpful to lead a comprehensive picture of the d electron system.

We carefully tested possible synthesis routes aiming the Na-based pyrochlore, and very recently we found that an entire exchange between K in KOs_2O_6 and Na is feasible under a certain condition in vacuumed quartz tube. Indeed, we succeeded in synthesis of a high-quality polycrystalline sample of the Na-based pyrochlore for the first time, and the structure, the magnetic and the charge transport properties were revealed. Although the compound is fairly metallic in nature, an expected superconductivity was not observed (>2 K). We discuss possible reasons.

2. Experimental

We prepared the host compound KOs_2O_6 by a solid-state method from KO_2 (powder, Aldrich), OsO_2 (Os—84.0%, Alfa Aesar), and Os (99.9%, Aldrich) in a manner reported elsewhere [20]. Powders of KOs_2O_6 and $NaNO_3$ (99.9%, Wako) were mixed in a platinum container at the ratio 1 to 5 in weight. The mixture was

* Corresponding author. Superconducting Materials Center, National Institute for Materials Science, 1-1 Namiki, Tsukuba, Ibaraki 305-0044, Japan.
Fax: +81 29 860 4674.
E-mail address: SHI.Youguo@nims.go.jp (Y.G. Shi).

0022-4596/$ - see front matter © 2009 Elsevier Inc. All rights reserved.
doi:10.1016/j.jssc.2009.01.008

heated in an evacuated quartz ampoule at 330 °C for 7 days. The product was washed in water and dried at 100 °C for 1 h in air. An electron probe micro-analysis (EPMA) confirmed the qNa rich composition; 93% of K in the host was replaced by Na. The exchange steps were repeated in the same way, resulting in promotion of the exchange reaction. In addition, we observed visible OsO_4 inside of the ampoule, suggesting an overcharged reaction to some extent. The EPMA study of the product revealed the mean ratio of Na:K:Os = 1.418:0.025:2. Thus, we decided to label the compound as $Na_{1.4}Os_2O_6 \cdot H_2O$ hereafter (H_2O is discussed later). It appears that the Os valence is reduced to +5.3 from +5.5 (KOs_2O_6), if the oxygen composition is exactly stoichiometric, as a result of accommodation of the excess Na. We would state that the oxygen content was not measured by a thermo-gravimetric analysis (TGA) method because the highly toxic OsO_4 was expected to come out from the sample. We attempted TGA only below 200 °C.

Sample quality of the polycrystalline $Na_{1.4}Os_2O_6 \cdot H_2O$ was checked by a powder X-ray diffraction (XRD) method using Cu$K\alpha$ radiation in a commercial apparatus (RIGAKU, RINT 2200 V). The crystal structure of $Na_{1.4}Os_2O_6 \cdot H_2O$ was studied by a Rietveld method using synchrotron XRD data measured at room temperature in a large Debye–Scherrer camera at the BL15XU beam line of SPring-8 [21]. The data were collected between 5° and 60° at the 0.003° interval in 2θ. Incident beam was monochromatized at $\lambda = 0.65297$ Å; a capillary (Lindenmann glass, outer diameter was 0.2 mm) containing the sample was rotated during the measurement. The Rietveld analysis was performed with RIETAN-2000 [22].

An amount of the sample was mold into a pellet using a belt-type apparatus (6 GPa was applied without heating). The dense pellet (black in color) was obtained, and was subjected for charge transport measurements. Electrical resistivity (ρ) of the pellet was measured by a four-point method with a gage current in a range of 1–10 mA at frequency of 30 Hz in a commercial apparatus (Quantum Design, Physical Properties Measurement System). Electrical contacts on the four locations along the bar-shaped pellet were prepared by gold wires and silver paste. Specific heat (C_p) was measured by a time-relaxation method in the apparatus. Magnetic properties of the polycrystalline $Na_{1.4}Os_2O_6 \cdot H_2O$ were studied in a commercial magnetometer (Quantum Design, Magnetic Properties Measurement System).

3. Results and discussion

Fig. 1 shows the synchrotron XRD pattern analyzed by the Rietveld method. At beginning of the structural analysis, we used the crystallographic parameters of KOs_2O_6 (space group: *Fd*-3*m*) as initial parameters [23]. Coefficients for analytical approximation to the atomic scattering factors were taken from Ref. [24]. The pseudo-Voigt function of Toraya was used as a profile function [25]. The background was represented by a composite background function, i.e., 11th-order Legendre polynomial multiplied by a set of numerical values to approximate the background. Isotropic atomic displacement parameters, *B*, with the isotropic Debye–Waller factor represented as $\exp(-B_{iso}\sin^2\theta/\lambda^2)$ was assigned to all the sites. For the impurity of OsO_2, we refined only a scale factor and the lattice parameters, fixing its structure parameters; the mass percentage of OsO_2 was calculated to be 0.9%.

While we started on the assumption that Na atoms are only at the 8*b* site ($\frac{3}{8}$, $\frac{3}{8}$, $\frac{3}{8}$) like K atoms in KOs_2O_6, we found significant electron density not only at the 8*b* site but also at the 16*d* site ($\frac{1}{2}$, $\frac{1}{2}$, $\frac{1}{2}$) (see Figs. 2a and b). Na occupation factors (g_{Na}) and *B* converged as follows: $g_{Na} = 0.817(15)$ and $B = 13.7(5)$ Å^2 at the 8*b* site and $g_{Na} = 0.721(5)$ and $B = 2.56(9)$ Å^2 at the 16*d* site. Since the *B* at the 8*b* site was unreasonably large, we checked possible chemical species located in the cage. Through the analysis, a model with water at the 32*e* site (originated from the 8*b* site) was found to describe best the structure of the compound. The refined occupation factor of O2(H_2O) was $g_{O2} = 0.260(4)$ with $B(O2) = 0.9(3)$ Å^2. Because the occupation factor of this site cannot exceed $\frac{1}{4}$ (that is, the occupation factor of the corresponding 8*b* site cannot exceed 1) we fixed $g_{O2} = 0.25$ in the final refinement. The Na atoms at the 16*d* site were found to be slightly split from the 16*d* to 32*e* site. The composition deduced from the final refinement is $Na_{1.4}Os_2O_6 \cdot H_2O$, which is highly reminiscent of what was found for $KNbWO_6 \cdot H_2O$ and $KNbWO_6 \cdot 0.69D_2O$ [26]. Besides, TGA result supports the hydration, as a notable weight loss more than 3% was observed during the compound was held in argon at 200 °C overnight (reaction was not completed), suggesting the dehydration. Final lattice parameters, *R* factors, fractional coordinates, *B* parameters, and selected bond lengths and bond valence sums are summarized in Table 1.

Figs. 2a and b show, respectively, a schematic view of the crystal structure and an illustration of the two oxygen cages

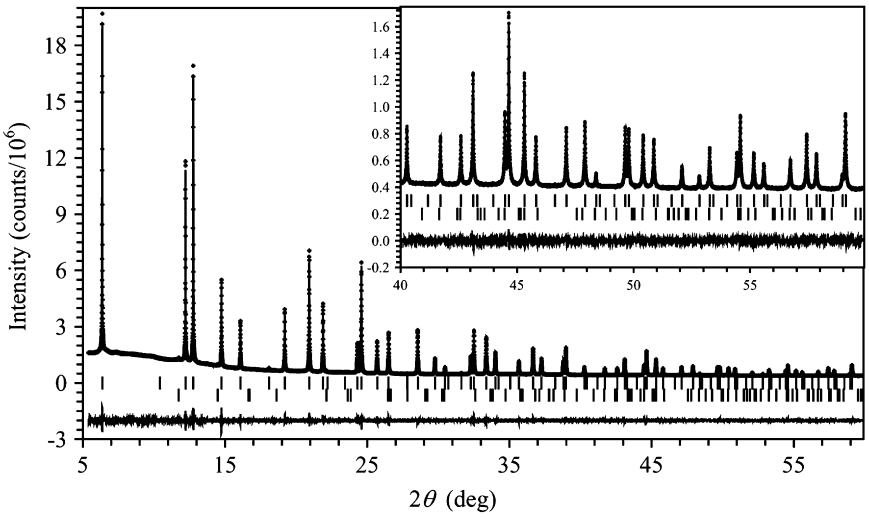

Fig. 1. Rietveld analysis of the synchrotron X-ray diffraction pattern for $Na_{1.4}Os_2O_6 \cdot H_2O$. Cross markers and solid lines show the observed and calculated powder diffraction profiles, respectively, and the difference is shown at the bottom. The positions of Bragg reflections are marked by ticks. Lower line of the ticks is for the impurity OsO_2. Inset shows an expansion of the pattern.

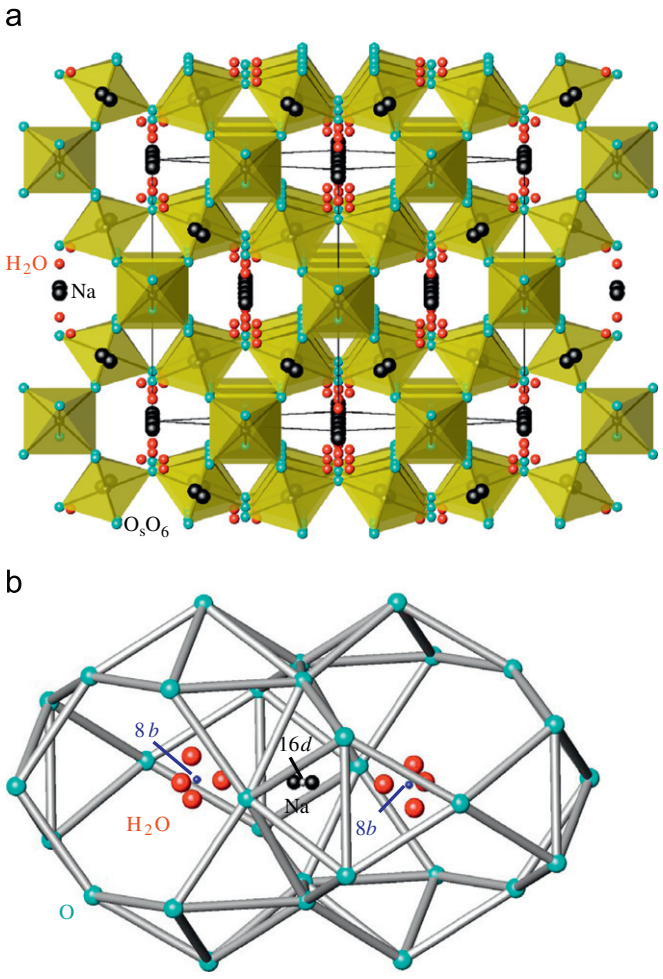

Fig. 2. (a) View of the crystal structure of $Na_{1.4}Os_2O_6 \cdot H_2O$ along the [110] direction. OsO_6 octahedra are shown. Large circles in channel are Na atom, and small circles are O2(H_2O) atom. (b) Two oxygen cages are combined around the 16*d* site. Na atoms and O2(H_2O) atoms are at the 32*e* site in the vicinity of the 16*d* site and the 8*b* site, respectively.

Table 1
Structure parameters of $Na_{1.4}Os_2O_6 \cdot H_2O$ determined by a synchrotron X-ray powder diffraction method at room temperature.

Site	Wyckoff position	*g*	*x*	*y*	*z*	*B* (Å^2)
Os	16*c*	1	0	0	0	0.150(4)
Na	32*e*	0.358(3)	0.4897(7)	$=x$	$=x$	1.60(15)
O1	48*f*	1	0.3194(2)	0.125	0.125	0.73(6)
O2(H_2O)	32*e*	0.25	0.4053(6)	$=x$	$=x$	0.6(3)

Space group is *Fd*-3*m* (no. 227) at origin choice 2, $Z=8$, $a=10.16851(1)$ Å, $V=1051.432(2)$ Å^3, and $D_{cal}=6.638\,g\,cm^{-3}$. *R* factors were $R_{wp}=2.46\%$, $R_p=1.58\%$, $R_B=2.12\%$, and $R_F=1.27\%$. Selected bond lengths are $d_{Os-O1}=1.931(1)$ Å (×6), $d_{Na-O1}=2.547(2)$ Å (×3), $d_{Na-O1}=2.605(4)$ Å (×3), and $d_{Na-O2}=2.255(14)$ Å; and the bond valence sum of NaO_7 is 1.03 [27]. Note that the bond valence sum of OsO_6 is unavailable since the R_0 parameter of Os^{5+} is uncertain [28].

around the nearest 8*b* sites, drawn based on the final solution. In the structure, Na atom resides on the 32*e* site that is in the vicinity of the 16*d* site (see Fig. 2b), while the O2 atom of the water molecule also resides on the 32*e* site that is in the vicinity of the 8*b* site. Although Na^+ and H_2O have the same number of electrons each, only the solution results in a reasonable sense. If Na is

Table 2
Superconducting transition temperatures (T_c), lattice parameters (*a*), the Sommerfeld coefficients (γ), and the Debye temperatures (Θ) of the related pyrochlore oxides.

Material	T_c (K)	*a* (Å)	γ (mJ mol^{-1} K^{-2})	Θ (K)	Reference
$Na_{1.4}Os_2O_6 \cdot H_2O$	–	10.16851(1)	21.4(1)	301.9(3)	This work
KOs_2O_6	9.5	10.0968(8)	76–110		[23]
$RbOs_2O_6$	6.3	10.1137(1)	40.4–44	325	[23,30,31]
$CsOs_2O_6$	3.3	10.1477(1)	39.0–40.0		[31]
$Cd_2Os_2O_7$	–	10.1651(4)	1.1–1.4	354–463	[15]
$Hg_2Os_2O_7$	–	10.228	21	230	[17,32]
$Cd_2Re_2O_7$	1	10.226(2)	26.5–30.2	285–458	[33,34]
$Cd_2Ru_2O_7$	–	10.129(1)	12.3	310	[34,35]

around the 8*b* site and H_2O is around the 16*d* site, the bond distances Na–O1 and H_2O–O1 become unreasonably long and short, respectively. It should be noted that the parameters g_{Na}, B_{Na}, and B_{O2} were refined simultaneously. Besides, the Na content estimated from g_{Na} was in good agreement with the EPMA result. The overall refinement converged readily to a fairly reasonable state, indicating that the OsO_6 framework is highly rigid with reasonable *B* for Os and O1 sites.

In the superconductor KOs_2O_6, K atoms locate at the 8*b* site, and nothing is at the 16*d* site [20]. The pyrochlore structure with the specific atom distribution is so called "β-type." On the other hand, K atoms locate near the 16*d* site in the pyrochlore $KNbWO_6 \cdot H_2O$, while H_2O is near the 8*b* site [26]. Thus, the hydrated compound is not categorized into the β-type, but the defect "regular"-type. A "regular" pyrochlore $A_2Tr_2O_7$ has *A* element at the 16*d* site and oxygen (O^{2-}) at the 8*b* site. Considering the varieties of the pyrochlore structure, the newly synthesized compound $Na_{1.4}Os_2O_6 \cdot H_2O$ should be categorized as a defect pyrochlore rather than a β-pyrochlore. Note that a structural model with Na at the 16*d* site and H_2O molecules near the 8*b* site was proposed for the Na-based tungsten oxide $NaNbWO_6 \cdot 0.5H_2O$, which is comparable with what we found for $Na_{1.4}Os_2O_6 \cdot H_2O$ [26].

Another remarkable feature found in the present study is about the lattice cell size. The cubic unit cell of $Na_{1.4}Os_2O_6 \cdot H_2O$ [$a=10.16851(1)$ Å] is larger than that of the other AOs_2O_6 (10.149 Å for $CsOs_2O_6$ [3], 10.114 Å for $RbOs_2O_6$ [2], and 10.099 Å for KOs_2O_6 [1]; see Table 2). Although Na is much smaller than the other *A* atoms, the excess Na and the hydration are probably responsible for the enlargement, as thoroughly discussed in Ref. [29].

Temperature dependence of magnetic susceptibility (χ) of the polycrystalline $Na_{1.4}Os_2O_6 \cdot H_2O$ was measured in zero-field cooling (ZFC) and field cooling (FC) conditions between 5 and 300 K. Applied magnetic field was fixed during each measurement at a magnitude between 1 and 70 kOe. The data in χ vs. *T* are shown in Fig. 3a. It appears that the magnitude of χ increases step by step with increasing the magnetic field over the whole temperature range, indicating a substantial magnetic background. In order to study further, we tried to measure χ beyond 300 K. It was, however, unsuccessful because the sample was chemically changed.

We also measured isothermal magnetization at various temperatures: the magnetization data are shown in Fig. 3b. The data clearly indicate a ferromagnetic contribution with small spontaneous magnetization of ~0.001 μ_B per Os, which is nearly temperature independent (<300 K). The observed ferromagnetic features are most likely due to a small amount of ferromagnetic impurities in the sample. It is reasonable to deem that the impurity is responsible also for the substantial background observed in χ vs. *T*. We thus repeated the sample preparation

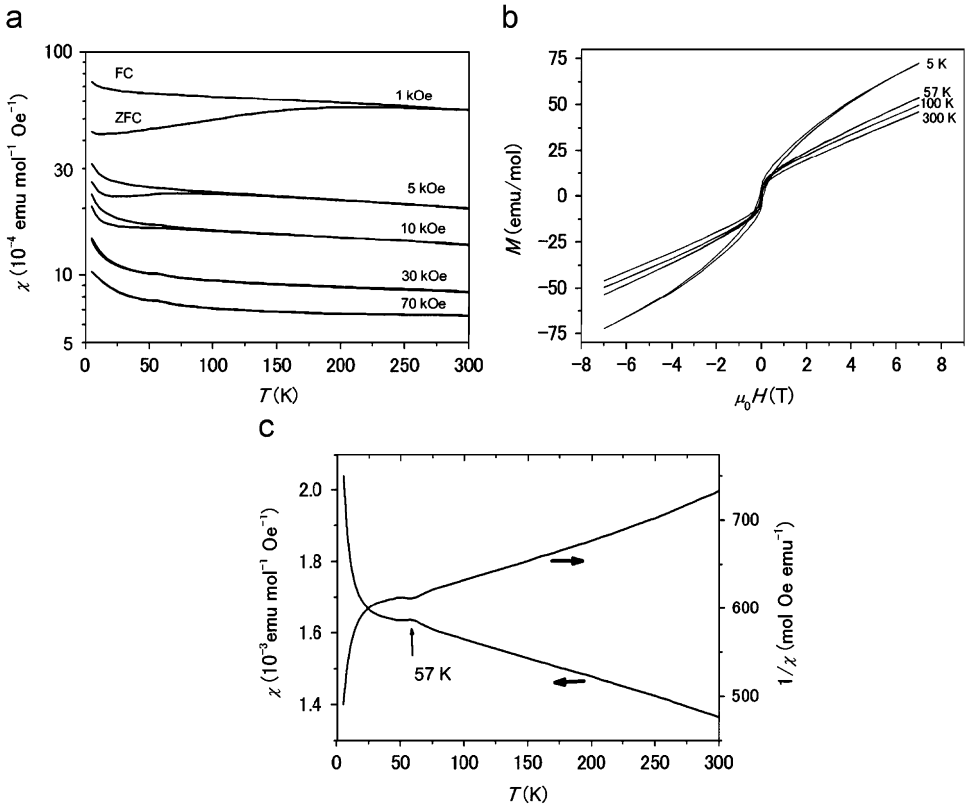

Fig. 3. (a) Temperature dependence of the magnetic susceptibility of the polycrystalline $Na_{1.4}Os_2O_6 \cdot H_2O$, (b) isothermal magnetization at various temperatures, and (c) an alternative plot of the 10 kOe data.

carefully to avoid the ferromagnetic incorporation. However, the magnetic background remained visible in all subsequent studies; although the XRD patterns are likely clean enough from impurity contributions. Hence, we should deem alternative possibilities: a parasitic ferromagnetism caused by some defects in the host is able to account for the magnetic anomaly, as thoroughly discussed for $Hg_2Os_2O_7$ and $Cd_2Os_2O_7$ [16,17]. A spin canting model proposed for Na_3OsO_5 is also possible to be responsible for the magnetic background [18]. In any case, further studies are necessary to evaluate the possibilities and to identify the primary origin, including such as a solid-state NMR study.

Fig. 3c shows $1/\chi$ vs. T of the 10 kOe data. As a Curie–Weiss (CW) feature is manifested, we applied the CW law to parameterize the linear part (>100 K). It should be kept in mind; however, that the applicability of the CW law to an itinerant system is not theoretically well justified, although in practice often yields useful results. Fits were conducted with and without a temperature-independent term χ_0. For $\chi_0 = 0$, the best fit yielded 2.84(2) μ_B/Os for the effective Bohr magneton, and $-1.17(2) \times 10^3$ K for the Weiss temperature, suggesting predominantly antiferromagnetic interactions. For $\chi_0 \neq 0$, the fit yielded 2.90(89) μ_B/Os and $-1.20(42) \times 10^3$ K at $\chi_0 = -3.0047(5) \times 10^{-5}$ emu mole^{-1}.

In $1/\chi$ vs. T, an additional magnetic anomaly is prominent at 57 K as marked. The anomaly is visible in the high magnetic field data (see Fig. 3a), while it is not in the low field data ($\leqslant 5$ kOe). Considering alike features of $Cd_2Os_2O_7$ and $Hg_2Os_2O_7$, which show anomaly at 227 K [15] and 88 K [17], respectively, the 57 K anomaly likely reflects an establishment of a long-range magnetic order. In order to confirm the hypothesis, we carefully measured magneto-charge transport of $Na_{1.4}Os_2O_6 \cdot H_2O$ over a wide temperature range through the anomaly temperature.

Because the ion-exchanged sample was loose powder, we prepared a dense pellet by a cold press method for the charge transport measurements. The powder was isotropically compressed at 6 GPa without heating. Fig. 4a shows temperature dependence of the electrical resistivity of the polycrystalline $Na_{1.4}Os_2O_6 \cdot H_2O$, measured with and without an applied magnetic field of 70 kOe. Over the whole temperature range between 2 and 300 K, fairly metallic characters such as a nearly T-linear dependence and a low resistivity ($\sim$1.2 mΩ cm at room temperature) are obvious. The residual resistivity ratio ($= \rho_{300\,K}/\rho_{2\,K}$) is moderate, 3.2. Inset to Fig. 4a shows differential curves of the resistivity data, $d\rho/dT$. It appears that the curves change those characters at $\sim$56 K, implying an association between the charge transport and the magnetic anomaly. Besides, the differential curves cut the zero-axis at $\sim$5 K, indicating a local minimum of the $\rho(T)$ curve. The weak Kondo effect-like feature is possibly due to interactions between charge carriers and localized magnetic moments probably caused by defects.

Over a wide temperature range, $\rho(T)$ is T-linear dependent (Fig. 4a), suggesting an exotic scattering mechanism [36]. To evaluate the possibility, we applied the Bloch–Gruneisen (BG) relation over the whole studied range, since the model often well describes conventional electron–phonon scattering in a metallic compound [37]. We used an analytical formula reduced from the BG function,

$$\rho(T) = \rho_0 + \left(\frac{c}{\Theta}\right)\left(\frac{T}{\Theta}\right)^5 \left(120\zeta(5) - \sum_{k=1}^{\infty} \exp(-ky) \times \left[y^5 + \frac{5}{k}y^4 + \frac{20}{k^2}y^3 + \frac{60}{k^3}y^2 + \frac{120}{k^4}y + \frac{120}{k^5}\right]\right),$$

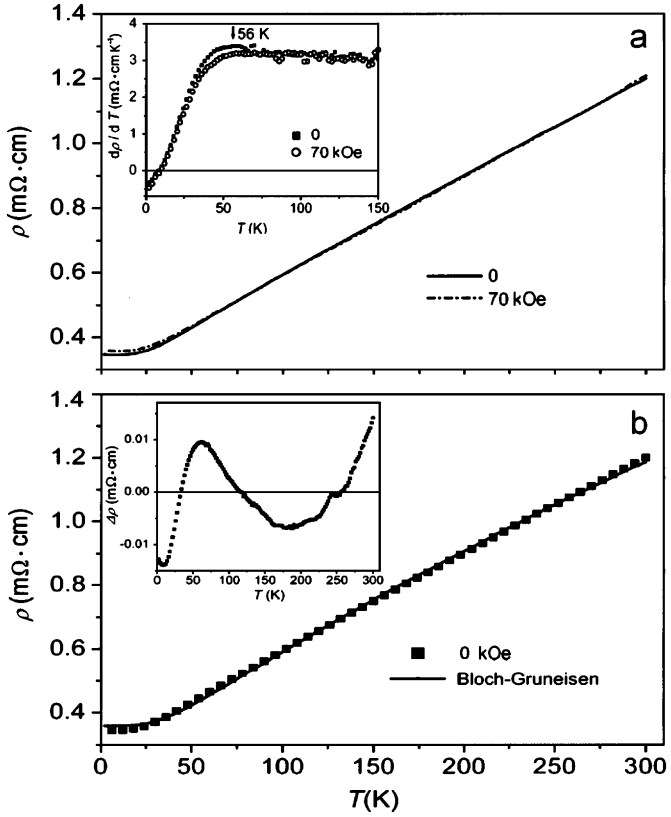

Fig. 4. (a) Temperature dependence of electrical resistivity of the polycrystalline $Na_{1.4}Os_2O_6 \cdot H_2O$ measured at $H = 0$ and 70 kOe. Top inset shows differential curves of the data. (b) The Bloch–Gruneisen function (solid curve) and the $H = 0$ data points. Bottom inset shows difference between those.

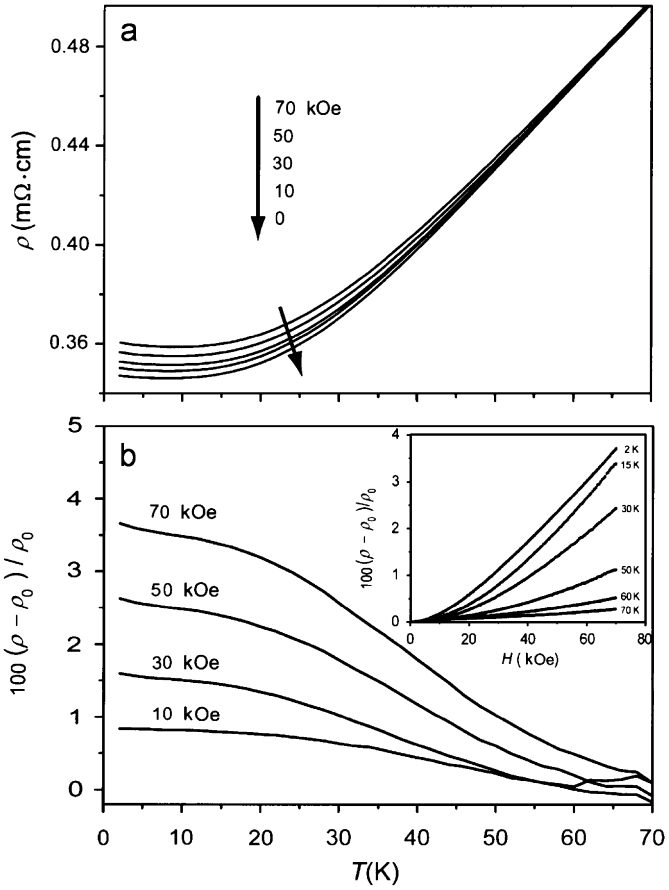

Fig. 5. (a) Field dependence of electrical resistivity of the polycrystalline $Na_{1.4}Os_2O_6 \cdot H_2O$ at low temperature and (b) the normalized plot. Inset shows the $\Delta\rho/\rho(0)$—H relation at various temperatures. Note that the $\Delta\rho/\rho(0)$ below ~70 K are positive.

where $\zeta(p) = \sum_{k=1}^{\infty} k^{-p}$ is the Riemann zeta function, $y = \Theta/T$, c is a constant, and Θ is the Debye temperature [37]. Following parameters were deduced from fit to the zero-field resistivity data by a least-squares method; $\rho_0 = 0.360(2)\,\mathrm{m\Omega\,cm}$, $c = 525(15)\,\mathrm{m\Omega\,cm\,K^{-1}}$, and $\Theta = 211(3)\,\mathrm{K}$ (the fit is shown in Fig. 4b). The difference, $\Delta\rho = \rho_{exp} - \rho_{cal}$, is shown in the inset to Fig. 4b, demonstrating a drop at ~60 K. Although the drop occurs in the vicinity of the magnetic anomaly temperature 57 K, it is, however, unlikely due to a magnetic origin because the result $\rho_{exp} < \rho_{cal}$ dose not match with any magnetic scattering models even qualitatively. Besides, a comparable magnitude of change is seen between 200 and 300 K, suggesting a statistical error size. Thus, the origin of the drop cannot be assigned solely to the magnetic anomaly. At the end of the analysis, we reached a conclusion that phonon scattering is dominant in the charge transport, and a possible magnetic scattering is fairly weak even in low temperature.

We analyzed the resistivity data measured in 70 kOe; however, a remarkable difference was not obvious: a comparable result $\rho_0 = 0.369(2)\,\mathrm{m\Omega\,cm}$, $c = 600(19)\,\mathrm{m\Omega\,cm\,K^{-1}}$, and $\Theta = 227(4)\,\mathrm{K}$ was attained, suggesting a predominant phonon scattering. We also tested another practical formula reduced from the BG relation [38], and we reached comparable results and the same conclusion.

Meanwhile, small degree of positive magnetoresistance (MR) was found at the low temperature limit as shown in Fig. 4a. We focused our attention on the MR. Fig. 5a shows a magnetic field dependence of $\rho(T)$: degree of MR increases with increasing magnitude of the magnetic field. Fig. 5b shows a normalized plot of the data, indicating that the MR changes toward constant on cooling (approaching to +3.7% at 70 kOe). Field dependence of MR was further studied at several temperature points, and the data are shown in the inset to Fig. 5b. The MR emerges at nearly the magnetic anomaly temperature, and changes monotonically over the whole field range, suggesting that the MR is coupled with the magnetic anomaly at 57 K.

We measured C_p of $Na_{1.4}Os_2O_6 \cdot H_2O$ to study the magnetism further. The C_p data are plotted in the top panel of Fig. 6. Over the whole temperature range from 2 to 300 K, C_p changes monotonically without anomaly: an expected peak near the magnetically characteristic temperature 57 K was not detected. Although a small amount of magnetic impurity can account for the magnetic anomaly, an unusual magnetic transition without a C_p anomaly is also possible to be responsible for the anomaly, as intensively discussed for $Hg_2Os_2O_7$ [17]. In addition, an unconventional metallic magnetism suggested for such as $LaCrSb_3$ could also be responsible for the observed C_p and the magnetism [39]. In order to make clear magnetic nature of $Na_{1.4}Os_2O_6 \cdot H_2O$, we measured C_p in a magnetic field of 70 kOe. The data are plotted in the main panel of Fig. 6 along with the zero-field data. The plots, however, indicate no remarkable field dependence over the temperature/field range.

For a comparison, C_p of the superconductors KOs_2O_6 and $RbOs_2O_6$ are plotted in Fig. 6 (the data are taken from Ref. [23]). The comparison manifests absence of a bell-shaped feature in $Na_{1.4}Os_2O_6 \cdot H_2O$. As discussed in Ref. [23], the bell-shaped contribution is well characterized by a linear combination of the Debye and the Einstein models: the Einstein part is primarily responsible for the distinct temperature dependence which may be caused by an anharmonic lattice contribution due to the A-atom rattling [23]. We thus tried to fit the data of

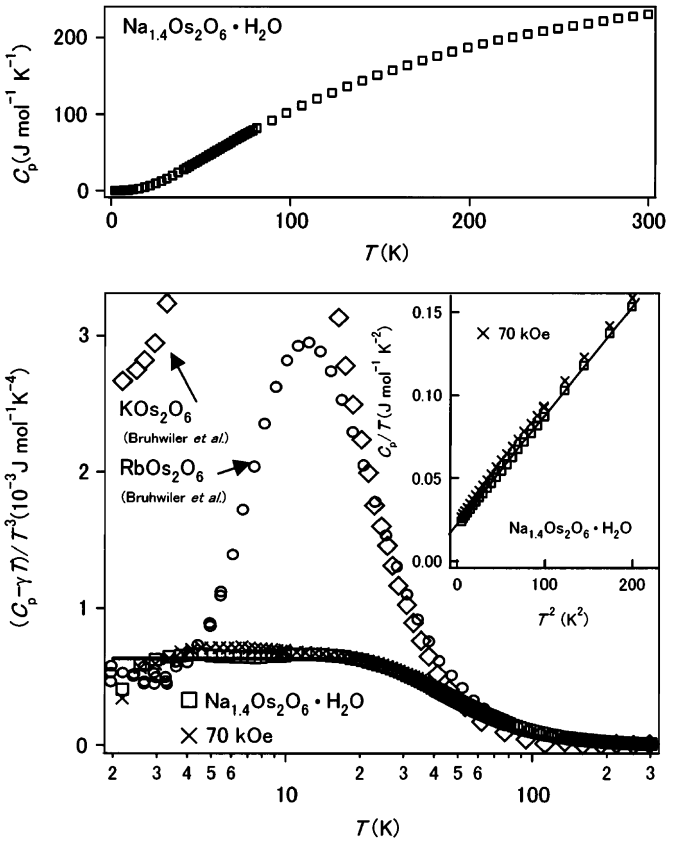

Fig. 6. Heat capacity of $Na_{1.4}Os_2O_6 \cdot H_2O$ at $H = 0$ and 70 kOe. The upper panel shows C_p vs. T between 2 and 300 K. The main panel shows a comparison of the lattice heat capacity $(C_p - \gamma T)/T^3$ with those of KOs_2O_6 and $RbOs_2O_6$ (the data are taken from Ref. [23]). The inset shows C_p/T vs. T^2 for $Na_{1.4}Os_2O_6 \cdot H_2O$.

$Na_{1.4}Os_2O_6 \cdot H_2O$ in the same manner, and found that the Debye part exclusively accounts for the C_p feature in a reasonable sense without the Einstein part. The solid curve is the best fit using only two variable parameters: the Debye temperature was 228 K and the density was 11.6 modes per the mole. The lack of the Einstein part in $Na_{1.4}Os_2O_6 \cdot H_2O$ accords with what was found in the structural analysis: the Na rattling is disabled because $Na_{1.4}Os_2O_6 \cdot H_2O$ crystallizes in rather a regular pyrochlore than a β-pyrochlore structure.

A low temperature part ($T \ll \Theta$) of C_p/T vs. T^2 is plotted in the inset to Fig. 6. An expected feature $C_p = \gamma T + \beta T^2$ is clearly seen, in which γ is the Sommerfeld coefficient and β is a coefficient including the Debye temperature. A line fit to the data by a least-squares method (shown as a solid line) yielded $\Theta = 301.9(3)$ K and $\gamma = 21.4(1)$ mJ mol^{-1} K^{-2}. It appears that the γ is smallest among the compounds of AOs_2O_6 (see Table 2), while the Θ is comparable, indicating that enhancement of the charge carrier mass is unremarkable in $Na_{1.4}Os_2O_6 \cdot H_2O$.

4. Conclusions

We achieved an entire ion exchange in KOs_2O_6. The Na-based Os oxide pyrochlore was synthesized for the first time and its structure, magnetic, and electrical properties were studied. The compound does not turn into a superconducting state ($\geqslant$2 K) against our expectation that the Na substitution increases T_c. The data suggest several reasons: (1) the compound does not crystallize into a β-pyrochlore but a defect "regular"-pyrochlore, (2) the Os valence is +5.3, which is lower than the common state of +5.5 of the superconductors AOs_2O_6 (A = Cs, Rb, and K), and (3) the compound is substantially hydrated. Although a very recent work suggested that small degree of hydration does not kill superconductivity in KOs_2O_6, our sample is, however, a non-superconductor ($\geqslant$2 K) probably because it is much highly hydrated: density of H_2O molecules inside is greater than 10 times than that of the hydrated superconductor $KOs_2O_6 \cdot nH_2O$ ($n < 0.1$) [40]. Considering the local structure environment, the hydration probably causes the Na-site shift from the 8*b* to the 16*d*, preventing Na rattling, as discussed in the hydrated KOs_2O_6 [23,26,40]. The hydration likely plays a pivotal role to destroy the superconducting state.

Because all the probable reasons mentioned above are caused by the excess Na and the hydration, we investigated more than 10 pieces of preliminary samples prepared under different conditions, which may have various Na/water quantities. We found, however, none of those shows superconductivity down to 2 K.

The compound $Na_{1.4}Os_2O_6 \cdot H_2O$ shows a magnetic anomaly at 57 K without a visible anomaly in C_p. The anomaly is coupled with MR (+3.7% at 2 K in the presence of 70 kOe). A magnetic transition without manifest change in magnetic entropy, as discussed for $Hg_2Os_2O_7$ and $LaCrSb_3$ [17,40], likely accounts for the anomaly. Because a possibility of influence from an undetected magnetic impurity on the data still remains, further efforts are needed to study the magnetic nature of $Na_{1.4}Os_2O_6 \cdot H_2O$.

Acknowledgments

We would like to thank Drs. R.W. Li, T. Kolodiazhnyi, and Z. Hiroi for helpful discussions. This research was supported in part by World Premier International Research Center (WPI) Initiative on Materials Nanoarchitectonics from MEXT, Japan, Grants-in-Aid for Scientific Research (18655080, 20360012) from JSPS, Japan, the Murata Science Foundation, Kyoto, Japan, and the Futaba Memorial Foundation, Mobara, Japan.

References

[1] S. Yonezawa, Y. Muraoka, Y. Matsushita, Z. Hiroi, J. Phys. Condens. Matter 16 (2004) L9.
[2] S. Yonezawa, Y. Muraoka, Y. Matsushita, Z. Hiroi, J. Phys. Soc. Jpn. 73 (2004) 819.
[3] S. Yonezawa, Y. Muraoka, Z. Hiroi, J. Phys. Soc. Jpn. 73 (2004) 1655.
[4] M. Bruhwiler, S.M. Kazakov, N.D. Zhigadlo, J. Karpinski, B. Batlogg, Phys. Rev. B 70 (2004) 020503R.
[5] T. Schneider, R. Khasanov, H. Keller, Phys. Rev. Lett. 94 (2005) 077002.
[6] T. Muramatsu, N. Takeshita, C. Terakura, H. Takagi, Y. Tokura, S. Yonezawa, Y. Muraoka, Z. Hiroi, Phys. Rev. Lett. 95 (2005) 167004.
[7] G. Schuck, S.M. Kazakov, K. Rogacki, N.D. Zhigadlo, J. Karpinski, Phys. Rev. B 73 (2006) 144506.
[8] S. Manalo, H. Michor, G. Hilscher, M. Bruehwiler, B. Batlogg, Phys. Rev. B 73 (2006) 224520.
[9] Y. Kasahara, Y. Shimono, T. Shibauchi, Y. Matsuda, S. Yonezawa, Y. Muraoka, Z. Hiroi, Phys. Rev. Lett. 96 (2006) 247004.
[10] Z. Hiroi, S. Yonezawa, Y. Nagao, J. Yamaura, J. Karpinski, Phys. Rev. B 76 (2007) 014523.
[11] A. Akrap, E. Tutis, S.M. Kazakov, N.D. Zhigadlo, J. Karpinski, L. Forro, Phys. Rev. B 75 (2007) 172501.
[12] I. Bonalde, R. Ribeiro, W. Braemer-Escamilla, J. Yamaura, Y. Nagao, Z. Hiroi, Phys. Rev. Lett. 98 (2007) 227003.
[13] M. Yoshida, K. Arai, R. Kaido, M. Takigawa, S. Yonezawa, Y. Muraoka, Z. Hiroi, Phys. Rev. Lett. 98 (2007) 197002.
[14] S. Erickson, S. Misra, G.J. Miller, R.R. Gupta, Z. Schlesinger, W.A. Harrison, J.M. Kim, I.R. Fisher, Phys. Rev. Lett. 98 (2007) 016414.
[15] D. Mandrus, J.R. Thompson, R. Gaal, L. Forro, J.C. Bryan, B.C. Chakoumakos, L.M. Woods, B.C. Sales, R.S. Fishman, V. Keppens, Phys. Rev. B 63 (2001) 195104.
[16] J. Reading, M.T. Weller, J. Mater. Chem. 11 (2001) 2373.
[17] M. Tachibana, H. Kawaji, T. Atake, Solid State Commun. 131 (2004) 745.
[18] K.M. Mogare, W. Klein, H. Schilder, H. Lueken, M. Jansen, Z. Anorg. Allg. Chem. 632 (2006) 2389.
[19] W.R. Gemmill, M.D. Smith, R. Prozorov, H.-C. Zur Loye, Inorg. Chem. 44 (2005) 2639.

[20] J. Yamaura, S. Yonezawa, Y. Muraoka, Z. Hiroi, J. Solid State Chem. 179 (2006) 336.
[21] M. Tanaka, Y. Katsuya, A. Yamamoto, Rev. Sci. Instrum. 79 (2008) 075106.
[22] F. Izumi, T. Ikeda, Mater. Sci. Forum. 321–324 (2000) 198.
[23] M. Bruhwiler, S.M. Kazakov, J. Karpinski, B. Batlogg, Phys. Rev. B 73 (2006) 094518.
[24] A.J.C. Wilson, E. Prince (Eds.), International Tables for Crystallography, vol. C, second ed., Kluwer, Dordrecht, The Netherlands, 1999, pp. 572–574.
[25] H. Toraya, J. Appl. Crystallogr. 23 (1990) 485.
[26] D.W. Murphy, R.J. Cava, K. Rhyne, R.S. Roth, A. Santoro, S.M. Zahurak, J.L. Dye, Solid State Ionics 18–19 (1986) 799.
[27] I.D. Brown, Acta Crystallogr. B 33 (1977) 1305.
[28] N.E. Brese, M. O'Keeffe, Acta Crystallogr. Sec. B 47 (1991) 192.
[29] G. Le Flem, R. Salmon, C. R. Seances Acad. Sci. Ser C Sci. Chim. 271 (1970) 1182.
[30] Z. Hiroi, S. Yonezawa, T. Muramatsu, J. Yamaura, Y. Muraoka, J. Phys. Soc. Jpn. 74 (2005) 1255.
[31] S.M. Kazakov, N.D. Zhigadlo, M. Bruhwiler, B. Batlogg, J. Karpinski, Supercond. Sci. Technol. 17 (2004) 1169.
[32] J. Reading, S. Gordeev, M.T. Weller, J. Mater. Chem. 12 (2002) 646.
[33] M. Hanawa, Y. Muraoka, T. Tayama, T. Sakakibara, J. Yamaura, Z. Hiroi, Phys. Rev. Lett. 87 (2001) 187001.
[34] K. Blacklock, H.W. White, J. Chem. Phys. 71 (1979) 5287.
[35] R. Wang, A.W. Sleight, Mater. Res. Bull. 33 (1998) 1005.
[36] J. Paglione, T.A. Sayles, P.-C. Ho, J.R. Jeffries, M.B. Maple, Nat. Phys. 3 (2007) 703.
[37] M. Deutsch, J. Phys. A Math. Gen. 20 (1987) 811.
[38] Y. Ishigaki, H. Mitsuhashi, Phys. Status Solidi A 99 (1987) K111.
[39] E. Granado, H. Martinho, M.S. Sercheli, P.G. Pagliuso, D.D. Jackson, M. Torelli, J.W. Lynn, C. Rettori, Z. Fisk, S.B. Oseroff, Phys. Rev. Lett. 89 (2002) 107204.
[40] R. Galati, C. Simon, C.S. Knee, P.F. Henry, B.D. Rainford, M.T. Weller, Chem. Mater. 20 (2008) 1652.